Results in Surfaces and Interfaces 18 (2025) 100462

Contents lists available at ScienceDirect

Results in Surfaces and Interfaces

journal homepage: www.elsevier.com/locate/rsurfi

Stacking classical-quantum hybrid learning approach for corrosion inhibition efficiency of N-heterocyclic compounds

Muhamad Akrom [a,*], Supriadi Rustad [a,**], Totok Sutojo [a], Wahyu Aji Eko Prabowo [a], Hermawan Kresno Dipojono [b,***], Ryo Maezono [c], Hideaki Kasai [d]

[a] Research Center for Quantum Computing and Materials Informatics, Faculty of Computer Science, Universitas Dian Nuswantoro, Semarang, 50131, Indonesia
[b] Quantum and Nano Technologies Research Group, Faculty of Industrial Technology, Institut Teknologi Bandung, Bandung, 40132, Indonesia
[c] School of Information Science, Japan Advanced Institute of Science and Technology, Ishikawa, 923-1292, Japan
[d] Department of Applied Physics, Osaka University, Suita, Osaka, 565-0871, Japan

ARTICLE INFO

Keywords:
Stacking model
Quantum machine learning
Corrosion inhibition
N-heterocyclic

ABSTRACT

This study introduces the stacking classical-quantum model (SCQM) as a novel approach to predicting N-heterocyclic compounds' corrosion inhibition efficiency (CIE). SCQM integrates classical models such as Multi-Layer Perceptron Neural Network (MLPNN) and Random Forest (RF) as base learners, with Quantum Neural Network (QNN) as the meta-learner. Experimental results demonstrate SCQM's superior performance with a coefficient of determination (R^2) value of 0.98 and root mean squared error (RMSE) of 0.92, outperforming classical models. Predictions of new derivatives PP1 and PP2 yielded CIE values of 95.39% and 94.05%, aligning with experimental results. The novelty lies in the hybrid framework's ability to leverage quantum feature maps, offering a groundbreaking method to explore anti-corrosion materials through quantum machine learning (QML).

1. Introduction

Metal corrosion, especially of iron and its alloys, presents a significant challenge in various industries. Efforts to mitigate this problem have focused on corrosion inhibitors, especially those derived from organic compounds, due to their non-toxic, environmentally friendly, cost-effective, and efficient nature (Jin et al., 2022), (Cui et al., 2022), (Akrom et al., 2023a), (Akrom, 2024a). Organic molecules containing heteroatoms (e.g., N, S, O, or P) and aromatic rings have been widely recognized for their high corrosion inhibition efficiency (Kozlica et al., 2021), (Kumar et al., 2022a), (Akrom et al., 2024a). N-heterocyclic compounds, such as pyrazole (Sayed et al., 2018), (Sarkar et al., 2021), pyrimidine (Luo et al., 2021), (Arrousse et al., 2020), (Rasheeda et al., 2018), (Echihi et al., 2023), (Khoutoul et al., 2014), pyridazine (Ghazoui et al., 2013), (Beniken et al., 2023), (Mrani et al., 2023), (Akrom et al., 2024b), (Akrom et al., 2024c), pyrrole (Verma et al., 2015), quinoline (Mehdi and Zandi, 2019), (Erdoğan et al., 2017), (Jiang et al., 2018), pyridine (Akrom et al., 2023b), and quinoxaline (Chauhan et al., 2020), (Masuku et al., 2023) have shown remarkable potential as corrosion inhibitors for iron and its alloys.

Experimental techniques such as gravimetry and electrochemical methods are commonly used to assess these compounds' corrosion inhibition efficiency (CIE). Although reliable, these methods are resource-intensive, time-consuming, and expensive (Akrom et al., 2023c), (Ben Seghier et al., 2022), (Alamri and Alhazmi, 2022), (Sutojo et al., 2023). To address these challenges, computational approaches such as density functional theory (DFT) and quantitative structure-property relationship (QSPR) modeling have attracted attention (Verma et al., 2020), (Verma et al., 2021), (Saranya et al., 2016), (Akrom et al., 2023d). DFT provides molecular-level insights into quantum chemical properties (QCP), while QSPR models use machine learning (ML) techniques to predict inhibitor performance (Beltran-Perez et al., 2022), (Quadri et al., 2022a), (Kumar et al., 2022b), (El Assiri et al., 2020a), correlating molecular characteristics with CIE (Toropov and Toropova, 2020), (Belghiti et al., 2019), (Budi et al., 2024), (Herowati et al., 2024a).

Our previous QSPR model using classical ML successfully predicted the CIE of diazine derivatives with good accuracy (85.02%–94.99%) compared to experimental values (Akrom et al., 2023e). However,

* Corresponding author.
** Corresponding author.
*** Corresponding author.
E-mail addresses: m.akrom@dsn.dinus.ac.id (M. Akrom), srustad@dsn.dinus.ac.id (S. Rustad), dipojono@itb.ac.id (H.K. Dipojono).

https://doi.org/10.1016/j.rsurfi.2025.100462
Received 29 November 2024; Received in revised form 24 January 2025; Accepted 18 February 2025
Available online 20 February 2025
2666-8459/© 2025 The Authors. Published by Elsevier B.V. This is an open access article under the CC BY-NC license (http://creativecommons.org/licenses/by-nc/4.0/).

classical approaches face limitations in capturing the complexity of quantum phenomena governing molecular interactions. Recognizing this, quantum machine learning (QML) has emerged as a promising alternative (Putra et al., 2019), (Agrawal and Choudhary, 2019), (Lim and Chi, 2019), (Akrom, 2024b), combining quantum computing principles with ML to extract deeper patterns and subtle correlations in complex quantum data (Ciliberto et al., 2018), (Cong et al., 2019), (Rosyid et al., 2024), (Benedetti et al., 2019), (Mitarai et al., 2018), (Grant et al., 2018), (Schuld and Killoran, 2019), (Zhu et al., 2019), (Havlíček et al., 2019), (Schuld et al., 2020), (Alcazar et al., 2020), (Herowati et al., 2024b). In this study, we propose a hybrid stacking learning framework that combines classical models, such as Multi-Layer Perceptron Neural Network (MLPNN) and Random Forest (RF) as base learners, with Quantum Neural Network (QNN) as meta-learners, namely Stacking Classic-Quantum Model (SCQM). Leveraging QML, this proposed model improves the predictive accuracy of CIE for N-heterocyclic compounds by representing molecular features in quantum states, which enables better modeling of nonlinear relationships. This work is a pioneering effort in applying QML to QSPR modeling for corrosion inhibitors, offering a scalable and efficient tool to advance materials informatics in corrosion prevention. The approach breaks new ground by demonstrating QNN's ability to synergize with classical learners, offering a pioneering application of QML in predicting and designing corrosion inhibitors.

2. Methods

2.1. Basic quantum computing

The quantum computation and information field has rapidly grown in the past two decades, leveraging principles from quantum mechanics for information processing and storage. Quantum computers use quantum bits (qubits) that can exist in multiple states simultaneously due to superposition, allowing for the simultaneous processing of numerous possibilities. Entanglement, a fundamental concept in quantum computing, enables interconnectedness among qubits, facilitating faster problem-solving than classical computers (Gupta et al., 2022), (Suzuki and Katouda, 2020), (Akrom et al., 2024d). Quantum gates manipulate qubits, performing superposition, entanglement, and interference, making computations infeasible for classical computers. Quantum computing has the potential to revolutionize fields such as cryptography, drug discovery, optimization, and material science (Ma et al., 2023), (Alhayani et al., 2023), (Deng et al., 2023), (Pyrkov et al., 2023).

The central and fundamental attribute defining the quantum state of a qubit is superposition, elegantly expressed as $|\psi\rangle = \alpha|0\rangle + \beta|1\rangle$, with $|\psi\rangle$ denotes the quantum states of the qubit while $|0\rangle$ and $|1\rangle$ are well known as computational basis states and form an orthonormal basis in a two-dimensional Hilbert space. The coefficients α and β are the amplitudes of a qubit in a superposition state, where the probabilities of a qubit being in states $|0\rangle$ and $|1\rangle$ are $|\alpha|^2$ and $|\beta|^2$, respectively. It's important to note that $|\alpha|^2 + |\beta|^2 = 1$, as the total probability must sum to 1. These coefficients can encompass complex values, allowing the qubit to exist in a complex linear combination of $|0\rangle$ and $|1\rangle$. This fundamental property of superposition in quantum mechanics empowers qubits to embody multiple values concurrently, showcasing the computational prowess of quantum computing (Brown and Zhuang, 2023), (Biamonte et al., 2017a), (Akrom et al., 2024e). Like classical logic gates manipulating classical bits, quantum computing employs unitary transformations, or quantum gates, to convert qubits from the ground to a superposition state. Examples include Hadamard (H), Pauli (P), and Rotation (R) gates. Applying the Hadamard gate transforms $|0\rangle$ and $|1\rangle$ qubits into superposition states, assuming the basis is $\{|0\rangle, |1\rangle\}$. A multi-qubit system with n qubits represented by the tensor product of n single-qubit states, encompassing 2^n basis states. This range spans $|00\ldots00\rangle$ to $|11\ldots11\rangle$, representing all possible quantum states for the n qubits (Kwak et al., 2021a), (Xia and Kais, 2019).

In the realm of quantum gates, the classical NOT gate, also known as a bit-flip operator, aligns with the Pauli-X gate. This gate switches the states $|0\rangle$ to $|1\rangle$ and $|1\rangle$ to $|0\rangle$. Another type of gate is the rotation gate, denoted as $R_x(\theta)$, $R_y(\theta)$, and $R_z(\theta)$, which rotates the qubit around the x, y, and z axes at specified angles (θ), constituting the gate parameters. While single-qubit gates like H, Pauli, and R gates operate on one qubit as input, there exist gates requiring two or more qubits for their functioning. Examples include Ising coupling gates (e.g., XX and ZZ gates) and Controlled Not (CNOT or CX) gates (Aishwarya et al., 2020), (Kwak et al., 2021b). The CX gate, acting as a switch in quantum circuits, uses one control qubit to determine whether the NOT gate applies to the target qubit, establishing correlations and enabling quantum entanglement. In a two-qubit configuration, observations of the qubits are interdependent. Quantum circuits, formed by a sequence of gates, are the foundation for quantum computation and information processing (Mishra et al., 2021), (Sagingalieva et al., 2023), (Akrom et al., 2025).

2.2. Proposed SCQM framework

The framework shown in Fig. 1 illustrates the proposed approach, namely SCQM, primarily focusing on integrating classical and quantum learning methods in a stacking learning approach. Data is explored through Exploratory Data Analysis (EDA) to understand data patterns followed by outlier handling and normalization to suit model needs. After that, the data is divided into a train set and a test set. During training, the K-Fold cross-validation technique is used on the training set to evaluate the performance of the base learner more generally. Two classical learning models based on neural networks and ensembles, MLPNN and RF, are used as base learners. The output of both base learners is in the form of predictions that will be used as input for the meta-learner. The meta-learner model, namely QNN, is built with encoding circuits and quantum structures (ansatz). Quantum Feature Map encodes data from base learners into quantum representations, while ansatz is applied to quantum data to capture non-linear relationships further. QNN, as a meta-learner, will process this quantum representation to make final predictions. All models, both base and meta learners, are optimized to obtain the best parameters to maximize performance. The trained model is evaluated on the test set using various evaluation metrics. The final predictions generated from this SCQM approach combine the strengths of classical and quantum models. In this proposed SCQM approach, base learners (MLPNN and RF) act as an initial step to capture general patterns. In contrast, QNN, as a meta-learner, improves the prediction by utilizing more complex quantum representations. In this case study, QNN is expected to provide advantages in handling further non-linear relationships, allowing a more adaptive model to complex data such as corrosion inhibition efficiency.

2.3. Dataset

Our research began with creating a data collection of 195 N-heterocyclic derivative chemicals. This data set was meticulously curated by merging information from many derivative compound data sets, all of which were gathered from published literature relating to corrosion inhibitor performance tests (Alamri and Alhazmi, 2022), (Obot and Umoren, 2020), (Quadri et al., 2022b), (Camacho-Mendoza et al., 2022), (Quadri et al., 2022c), (Ser et al., 2020a), (Liu et al., 2019), (El Assiri et al., 2020b). As many as 11 QCPs are used as input features (independent variables), while the CIE values are used as targets (dependent variables). The QCPs are closely related to the CIE, which is a significant factor in the search for effective anti-corrosion materials (Beltran-Perez et al., 2022), (Camacho-Mendoza et al., 2022). They are energy of the highest occupied molecular orbital (HOMO) and lowest unoccupied molecular orbital (LUMO), energy gap (ΔE), ionization potential (I), electron affinity (A), global hardness (η), global softness (σ), electronegativity (χ), dipole moment (μ), electrophilicity (ω),

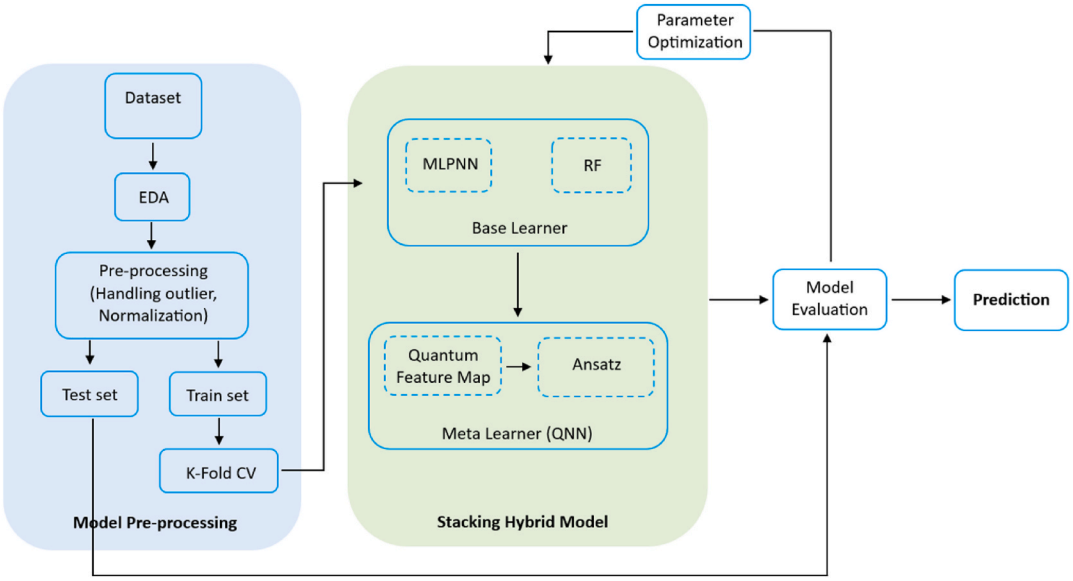

Fig. 1. Proposed SCQM frameworks.

fraction of electrons transferred (ΔN), and total energy (TE) These QCPs are calculated using DFT and the Koopmans method. At the same time, the CIE values are obtained from experimental studies.

2.4. EDA

EDA is a critical preliminary phase in data-driven analysis methodologies, addressing challenges like duplicate entries, imbalanced data, correlated features, missing values, and outliers. In pre-processing, EDA involves descriptive statistical analysis, computing metrics like mean, median, quartiles, and standard deviation to understand data characteristics (Linden and Marquis, 2023), (Ibarra-Vazquez et al., 2023), (Al Azies et al., 2024). Correlation analysis, using tests like the Wald test, assesses the impact of features on the target variable, revealing relationships among variables for predictive modeling. EDA insights contribute to model development assumptions and guide subsequent data processing stages, serving as a valuable tool for informed decision-making in the analytical pipeline (Abban et al., 2023), (Calafat-Marzal et al., 2023), (Rustad et al., 2024).

2.5. Data normalization

Feature scaling techniques are crucial for normalizing data, especially in datasets with varying scales or sensitivity issues, which are standard in large or differently scaled datasets (Ahsan et al., 2021), (Akrom et al., 2024f). Among these techniques, Robust-Scaler stands out for addressing outliers. Outliers are data points significantly divergent from the majority. Robust-Scaler relies on the interquartile range (Q3 - Q1) to scale the data, exhibiting resilience against outliers by normalizing based on the central 50% of the data distribution. This approach makes the scaling process less sensitive to extreme values, emphasizing the more representative central data distribution. Robust-Scaler employs a specific formula to scale each feature within the dataset.

$$X_{scaled} = \frac{X - Q_1}{Q_3 - Q_1} \tag{1}$$

In this equation, X denotes the original value of a data point, Q_1 represents the first quartile (25th percentile) of the feature data, and Q_3 represents the third quartile (75th percentile).

2.6. Data division

The data is divided into a train set and a test set with a ratio of 80:20. During training, the K-fold cross-validation (KFCV) technique is applied to divide the data into a train set and a validation set to evaluate the robustness of the model through iterative training to achieve minimal statistical error (Botchkarev, 2019), (Trisnapradika et al., 2025). This approach reduces bias and variance by grouping the dataset into 5 folds, each serving as a test set in a separate iteration. KFCV ensures a balanced evaluation of the model performance, addressing the issues of bias and variance. The choice of the number of folds (k) affects the trade-off between statistical precision and computational efficiency. Common choices, such as k = 5 or k = 10, balance precision and computational feasibility, with the appropriate value of k depending on factors such as dataset size and feature complexity (Yuan et al., 2014).

2.7. Algorithms

The RF method uses random feature selection and bagging (bootstrap aggregating) to build multiple decision trees. Combining the projections from each tree produces predictions. A random portion of the training dataset and a random subset of the characteristics taken into account at each node during tree construction are used to develop decision trees. In the end, and typically in the context of regression problems, the final prediction is obtained by averaging the predictions of all trees. The basic idea behind RF is to create a diverse ensemble of trees, each trained on a different subset of data and characteristics, and then combine their predictions to get a more reliable and accurate collective forecast. Depending on the objective, the forecast, represented as $F(x)$, obtained from N decision trees is usually calculated by voting or averaging.

$$\boldsymbol{F}(\boldsymbol{x}) = \frac{\mathbf{1}}{\boldsymbol{N}} \sum_{i=1}^{\boldsymbol{N}} \boldsymbol{F}_i(\boldsymbol{x}) \tag{2}$$

In the context of RF, the forecast from the ensemble's i-th tree is denoted by F(x). Ensemble averaging is essential in RF to reduce variation and improve the model's generalization ability.

MLPNN is an artificial neural network consisting of one input layer, one or more hidden layers, and one output layer, all fully connected. The network generates predictions by processing input data through layers of interconnected neurons, where each neuron applies an activation function to a weighted sum of its inputs. The network is trained using

backpropagation, a supervised learning technique that iteratively adjusts weights to minimize prediction error based on a predefined loss function. The basic principle behind MLPNN lies in learning a complex nonlinear mapping from input features to target outputs by optimizing the network's weights and biases. Each layer transforms the data into an increasingly abstract representation, allowing the model to capture complex patterns in the data set. The final prediction, $F(x)$, is obtained from the output layer, which incorporates the information processed through the hidden layers. In MLPNN, $F(x)$ represents the predicted value for input x. Iterative weight updates during training are essential to reduce error and improve the model's generalization of unseen data. This structure allows MLPNN to excel at classification and regression tasks across various domains.

$$\boldsymbol{F}(\boldsymbol{x}) = \boldsymbol{\phi}\left(\sum_{j=1}^{h} \boldsymbol{w_{jk}} \boldsymbol{a_j} + \boldsymbol{b_k}\right) \tag{3}$$

where h is the number of neurons in the hidden layer, w_{jk} is the weight between hidden neuron j and the output neuron k, b_k is the bias for the output neuron k, ϕ is the activation function, such as sigmoid, ReLU, or softmax depending on the task.

QNN is designed as in Fig. 2. The proposed QNN comprises three phases, as depicted in Fig. 2 (colored in blue, green, and yellow). Eleven qubits (q_0, q_1, …, q_{10}) represent classical features of QCP denoted as ψ_0, ψ_1, …, ψ_{10}. Each qubit initializes as a quantum ground state $|0\rangle$. The classical input data ψ undergoes conversion into quantum states $|\psi\rangle$ through a coding mechanism, employing variational encoding techniques like H gate followed by Ry gate. This process, represented in blue, involves quantum feature mapping, converting classical features into quantum state representations within Hilbert space, and creating rotations corresponding to input vector values. This encoding enables the creation of quantum superposition among qubits, allowing them to exist in multiple states simultaneously (Elsedimy et al., 2023), (Abdulsalam et al., 2023). Different gates can be chosen for input encoding to create diverse quantum state representations.

The phase in green represents a simple parametrized circuit framework employed to train the neural network model, comprising R_x, R_z, and CX gates. Within this framework, the individual rotation gates R_x and R_z contribute to a parametrized circuit featuring adjustable parameters denoted as $\delta = \theta$, where θ is any default rotation angle in radian. The CX gate enables the creation of quantum entanglement and fosters an inseparable connection between qubits. This enhances the robustness of the quantum representation for more intricate processing through complex quantum algorithms. The parametrized circuit layout has a circuit depth that scales linearly with the number of qubits, making it suitable for the specific problem formulation (Alsubai et al., 2023), (Narain et al., 2016), (Kavitha and Kaulgud, 2023). The rotation and CX gates implementation can be repeated or modified to create additional quantum circuits for subsequent layers.

As the anticipated value is obtained, the altered qubit state undergoes measurement (yellow). These measurements are then transformed into the suitable output data format through decoding (Wieder et al., 2021), (Biamonte et al., 2017b). The decoding process involves the conversion of qubit measurements into interpretable numerical values. After the quantum computation, measurements generate a probability distribution representing potential quantum states and their associated regression prediction values. The calculation of the regression prediction entails determining the expected value (EV) by multiplying each regression value with its corresponding probability and summing them as in equation (4).

$$EV = \sum_i P_i R_i \tag{4}$$

where P_i is the probability of the measurement result associated with the regression value R_i.

The quantum state is measured during training iterations to compute the cost function, an error metric (Abbas et al., 2021), (Qi et al., 2023). The optimization process involves a cost function ($F(x, y)$) depicted by equation (5), designed to model the training data for the decoder quantum gate. The cost function in QNN focuses on reducing the error between the predicted value (based on quantum expectation) and the target value with gradient-based optimization that exploits the unique properties of quantum circuits (Imanothai and Taetragool, 2023), (Kholili et al., 2023), (Ozpolat and Karabatak, 2023).

$$L = \frac{1}{N}\sum_{i=1}^{N}(y_i - \hat{y}_i)^2 \tag{5}$$

where N is the number of samples in the dataset, y_i is the actual target value for sample i, $\hat{y}_i$ it the predicted value for sample i.

2.8. Assessment metrics

Evaluation metrics like root mean square error (RMSE), mean absolute error (MAE), mean absolute deviation (MAD), mean absolute percentage error (MAPE), and coefficient of determination (R^2) are crucial for assessing model performance (Schuld and Killoran, 2019)–(Havlíček et al., 2019). They provide insights into the agreement between model predictions and tested data attributes. R^2 evaluates the proportion of predictable variance in the dependent variable, with a value close to 1 indicating high agreement. RMSE, MAE, and MAD indicate prediction errors, with lower values reflecting higher model accuracy (Putra et al., 2019), (Bafandeh et al.), (Pately et al., 2008).

$$R^2 = \frac{\sum_{i=1}^{n}(Y_i' - \overline{Y}_i)^2}{\sum_{i=1}^{n}(Y_i - \overline{Y}_i)^2} \tag{6}$$

$$RMSE = \sqrt{\frac{1}{n}\sum_{i=1}^{n}(Y_i' - Y_i)^2} \tag{7}$$

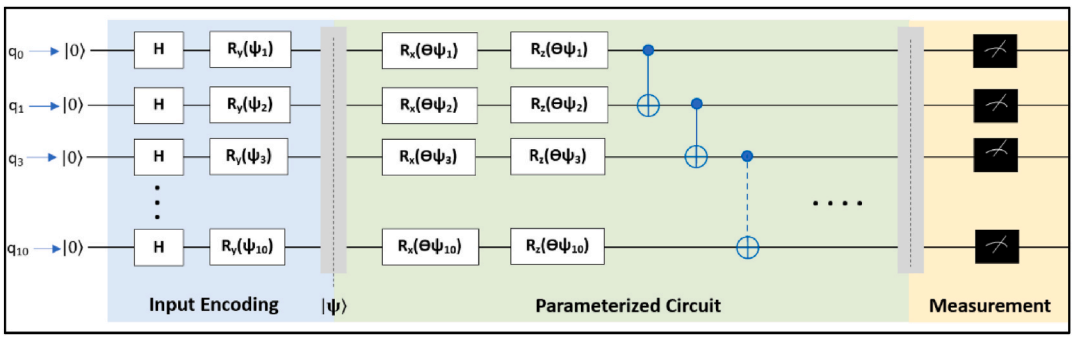

Fig. 2. The proposed QNN architecture with the input ψ and free parameter (δ = θ ψ).

$$MAE = \frac{1}{n}\sum_{i=1}^{n}|Y_i' - Y_i| \quad (8)$$

$$MAD = \frac{1}{n}\sum_{i=1}^{n}|Y_i' - \overline{Y}_i| \quad (9)$$

$$MAPE = \frac{1}{n}\sum_{i=1}^{n}\left|\frac{Y_i' - \overline{Y}_i}{Y_i}\right| \times 100\% \quad (10)$$

Here, n represents the number of samples, Y_i stands for the actual values, $\overline{Y}_i$ denotes the mean of the actual values and Y_i' represents the predicted values by the model. Collectively, these metrics provide a comprehensive evaluation of the model's performance and accuracy in predicting the outcomes of interest.

3. Results and discussions

3.1. EDA

EDA is a crucial preliminary phase in comprehending the statistical characteristics inherent within a dataset before delving into the modeling process. It plays a pivotal role in offering an initial insight into the distribution patterns and correlations existing between the target variable (such as CIE) and the various features (such as HOMO, LUMO, ΔE, I, A, η, σ, χ, ω, μ, and ΔN) in the dataset. By exploring and understanding these statistical properties through EDA, researchers gain valuable insights that form the foundation for constructing QSPR models. These models are specifically tailored to assess and predict the CIE of inhibitor compounds based on their molecular features. The knowledge obtained from EDA is a cornerstone for developing accurate and relevant QSPR models, enabling a better understanding of the relationships between molecular properties and the inhibitory performance of compounds.

The descriptive statistical analysis in Table 1 offers insightful information about the dataset, encompassing features, and the target variables. The descriptive statistics reveal diverse variances among the features. Specifically, the LUMO, A, and ΔE features exhibit notably high variances, indicating wider data dispersion from their respective means. Other features, namely μ, I, and ω, have significant variations. In contrast, features like HOMO, χ, η, σ, and ΔN demonstrate relatively low variances, implying a more concentrated data distribution around their means. Variance measures the extent of data points' spread from the mean, indicating that higher variance corresponds to more significant data variation. The target variable (CIE) displays considerable variance from its mean, implying significant variation within the dataset. This widespread from the average highlights the diverse nature of the target values in the dataset.

According to the Spearman correlation analysis presented in Fig. 3, notable positive and negative correlations exist between the QCP features and the CIE targets. Remarkably, none of the features exhibit a zero-correlation value, affirming the statistical presence of correlations for each feature. Furthermore, the observed P-value is remarkably low, roughly aligning with the commonly selected threshold of 0.05. This implies a high level of statistical significance for these associations. While these outcomes indicate a correlation between the features and the target variable, it's crucial to acknowledge that correlation does not inherently suggest causation. Nonetheless, comprehending the correlations and statistical significance of these features can aid in crafting predictive models or pinpointing pivotal parameters that influence corrosion protection. This holds significance in creating materials with attributes aimed at minimizing corrosion-induced damages.

Table 1
Descriptive statistic results for features and target.

Descriptors	Mean	Variance	Standard deviation
Features			
HOMO	−6.088	0.333	0.573
LUMO	−1.261	6.727	2.594
ΔE	4.853	7.533	2.745
M	4.042	5.386	2.321
I	5.043	4.414	2.101
A	1.043	6.646	2.578
X	3.604	1.662	1.289
H	2.566	1.842	1.357
Σ	0.399	0.252	0.502
Ω	2.138	5.242	2.290
ΔN	0.478	0.094	0.307
Target			
CIE	88.244	78.434	8.856

The results from the Wald test, as presented in Table 2, are crucial in determining the significance of the features' impact on the target variable within a regression model. The χ^2 statistic from the Wald test is 6.295, indicating the distance of the parameter estimate from zero. A more considerable χ^2 value signifies a stronger case for the features' significant effect or influence on the target variable. Moreover, the associated p-value obtained from the test is 0.039. Typically, a p-value below the conventional significance level of 0.05 implies compelling evidence to reject the null hypothesis, which assumes no effect or influence of the independent variables on the dependent variable. Therefore, a p-value of 0.039 suggests strong enough evidence to reject the null hypothesis, indicating the potential presence of a significant effect of the features on the target variable within the model tested. In summary, the Wald test outcomes imply the possibility of a notable impact of the features on the target variable within the model, emphasizing the potential significance of these features in influencing the target.

3.2. Model performance

To build an optimal model stacking framework, hyperparameter tuning is performed on each model, namely MLPNN and RF as base learners and QNN as meta learners. Hyperparameter tuning uses the GridSearchCV technique to identify optimal parameters. Table 3 presents the tuned parameters and their optimal results in this case. These optimization results ensure that each model provides maximum contribution in the model stacking framework, thus improving the overall performance in classification tasks.

The performance of QNN also shows its adaptability to different optimizer configurations. Fig. 4 illustrates the fluctuation of its performance as depicted by the R2 and RMSE values across different optimizers, namely Cobyla, RMSprop, and Adam. The average results depict the consistently stable performance of QNN amidst different optimization conditions; the average R2 is 0.968 (Standard Deviation = 0.008), and the average RMSE is 1.112 (Standard Deviation = 0.142). The low standard deviation indicates the consistency and stability of the QNN model across different optimizers. Despite slight variations in the measured results, the average R^2 and RMSE values remain within the range, indicating relevant predictions. This stability is key to ensuring that QNN can reliably function as a meta-learner in a model stacking framework. Thus, QNN contributes significantly to the overall model accuracy and demonstrates robustness to parameter changes, making it a critical component in developing prediction methods for reliable results in this case study.

In addition to classical parameter tuning, QNN adjusts the ansatz layer configuration to ensure optimal performance. These adjustments include the number of ansatz layers, as shown in Fig. 5. Competitive results are obtained using 6 layers, which offer a balance between complexity and quantum representation capability. The number of layers used significantly affects the performance evaluation of the QNN model. This finding underscores the importance of carefully selecting the number of layers to balance model complexity and generalization, which is essential for more accurate predictions in this context. These

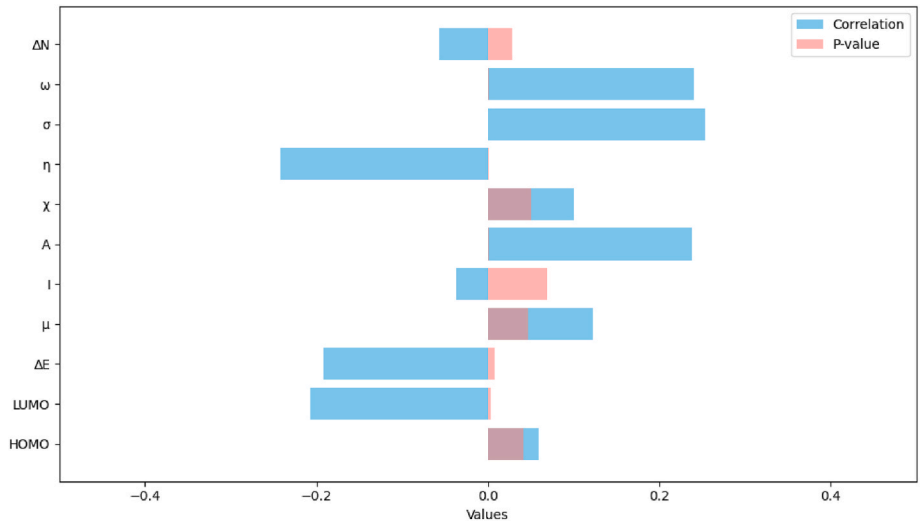

Fig. 3. Spearman correlation and p-value of features and target.

Table 2
Wald test results.

Chi-square (χ^2)	p-value
6.295	0.039

Table 3
Hyperparameter tuning for each base and meta-learner.

Model	Parameter	Values	Best Value
QNN	Batch size	16, 32, 64	32
	Learning rate	0.001, 0.01, 0.1	0.01
	Epoch	50, 100, 200	100
	Optimizer	Adam, Cobyla, RMSprop	Cobyla
	Safe margin	0.1, 0.5, 1	0.1
MLPNN	Batch size	16, 32, 64	32
	Learning rate	0.001, 0.01, 0.1	0.01
	Epoch	50, 100, 150	100
	Optimizer	Adam, Cobyla, RMSprop	Adam
	Dropout rate	0.1, 0.3, 0.5	0.3
	Hidden layer	1, 2, 3	2
	Neurons per layer	16, 32, 64	32
RF	Number of estimators	50, 75, 100	75
	Max depth	5, 10, 15	10
	Min samples split	2, 5, 10	2
	Min samples leaf	1, 2, 4	1

adjustments aim to improve the efficiency of the quantum circuit in capturing complex patterns from the data, thereby contributing significantly to the overall performance of the stacking model. This optimized parameter combination ensures that QNN can effectively act as a meta-learner in the proposed classification framework. This enhanced process is intended to improve the reliability and precision of QNN, potentially impacting prediction accuracy. This approach aligns with the general goals of achieving clear numerical representation, following quantum probability theory, normalizing results, strengthening error robustness, and maintaining interpretability in regression tasks.

The experimental results in Table 4 show that SCQM significantly outperforms classical models such as MLPNN and RF in the studied cases. Based on the evaluation metrics, SCQM achieves an R^2 value of 0.98, significantly higher than MLPNN (0.79) and RF (0.88). In addition, SCQM records the lowest RMSE, MAE, MAD, and MAPE values of 0.92, 0.64, 0.51, and 0.71, respectively, compared to MLPNN and RF. The superior performance of SCQM demonstrates the significant benefits of integrating QNN into the hybrid model stacking framework. QNN, as a

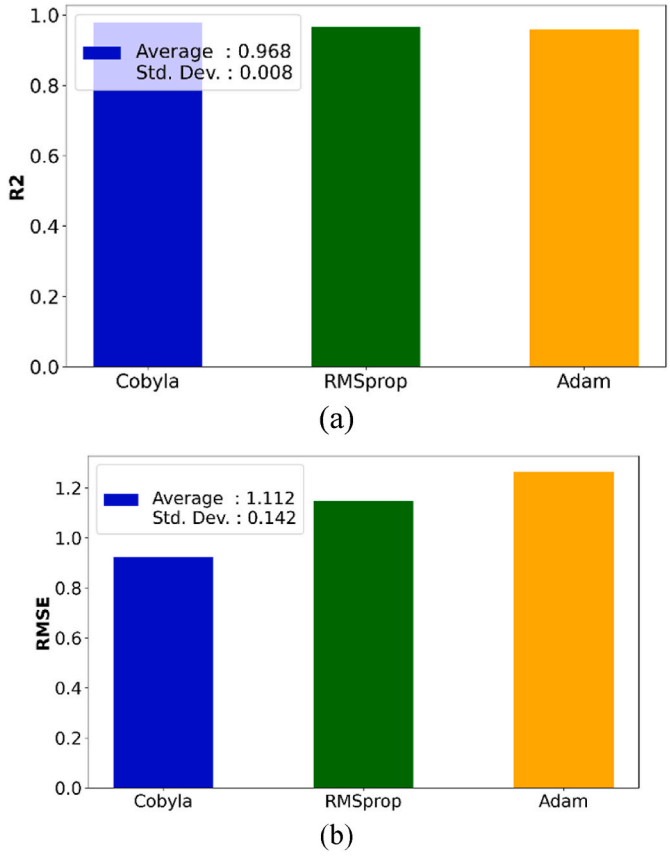

Fig. 4. Plots of average and standard deviation of (a) R^2 and (b) RMSE values for diverse optimizers of QNN.

meta-learner, can leverage the features generated by classical models and enhance the overall prediction capability through its capacity to capture complex relationships in the data. The stability and accuracy of QNN strengthen the stacking framework, making it more robust than individual models. This confirms that the SCQM approach can improve prediction performance and opens up new opportunities to leverage the advantages of quantum technology to enhance classical learning methods in this task.

The superiority of the SCQM, in contrast to the other two models, is

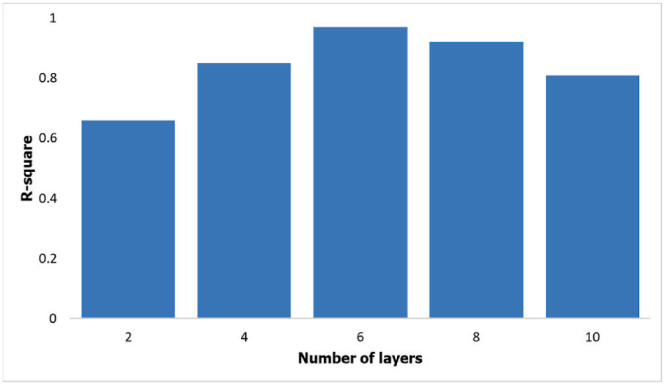

Fig. 5. QNN model performances under various layers.

Table 4
Model performances on N-heterocyclic dataset.

Model	R^2	RMSE	MAE	MAD	MAPE
MLPNN	0.79	3.02	2.40	2.23	2.64
RF	0.88	2.45	2.10	1.56	2.43
SCQM	0.98	0.92	0.64	0.51	0.71

further evidenced through the analysis presented in Fig. 6, encompassing both the scatter plot and residual error. In the scatter plot, crucial observation surfaces are found: the data points are broadly dispersed around the diagonal line. This alignment with the diagonal signifies that the model's predicted values closely align with the actual values, signifying the reliability and accuracy of the model's predictions. This close clustering around the diagonal line underscores the SCQM's capability to provide dependable predictions of the CIE values. When examining the residual error plot, a distinct pattern emerges: the data points exhibit a random and evenly distributed arrangement around the horizontal axis ($y = 0$). This evenly dispersed distribution suggests that the model's predictions showcase a consistent pattern without significant systematic bias. The absence of any discernible trend or pattern in the residual errors further reinforces the reliability and stability of the SCQM's predictions. The scatter plot and residual error analysis in Fig. 6 emphasize the SCQM's robustness in delivering accurate and consistent predictions, affirming its superiority in forecasting CIE values compared to the other models.

From comprehensive metric evaluation and data distribution analysis of prediction points, it can be concluded that the SCQM model consistently performs better than both classical RF and MLPNN models, showing higher accuracy and more minor prediction errors. In addition, the prediction error distribution displays a more even pattern and is closer to zero. The superior performance of the QNN model indicates its ability to understand complex patterns in N-heterocyclic inhibitor compound data, thereby ensuring more accurate and reliable predictions. The strength of this QNN model comes from its ability to capture complex molecular features, especially as they are influenced by quantum effects obtained from DFT calculations. Such capabilities allow it to account for quantum effects on inhibitor molecular properties, which conventional models such as MLPNN or RF can be challenging to capture. Its innovative approach, which integrates quantum computing principles into neural networks for molecular or quantum data analysis, opens up a lot of potential. This pioneering methodology may reveal previously undiscovered relationships between molecular structure and corrosion inhibitor properties, evading the understanding of classical models. In essence, SCQM stands as a promising, innovative approach to uncovering deeper insights and establishing new relationships between molecular structure and corrosion inhibitor properties, going beyond the limitations of conventional modeling techniques.

A fair and rigorous comparison between SCQM and classical models represented by MLPNN and RF has been performed using the same dataset, namely N-heterocyclic compounds. This comparison considers the best parameter configuration for each model. As mentioned earlier, the results show that the hybrid classical-quantum model outperforms the classical model alone in prediction accuracy and stability. It will be interesting to see the position of SCQM performance among the predictive abilities of different models applied across different datasets featuring N-heterocyclic derivatives found in the existing literature. These datasets include a variety of N-heterocyclic compounds: pyridazine, pyrimidine, pyridine-quinoline, and quinoxaline. The models used in this analysis include artificial neural networks (ANN), genetic algorithm-based ANN (GA-ANN), multilinear regression (MLR), RF, and MLPNN, with R2 and RMSE serving as the two main evaluation metrics. Each model was carefully fitted to a specific dataset, and their performance across these datasets is detailed in Table 5. A notable performance was observed in the SCQM model applied to the (proposed) N-heterocyclic dataset. Demonstrating an outstanding performance, the SCQM model exhibited an R2 of 0.98 and a very low RMSE of 0.92. This underscores the high precision of the model in predicting the properties of N-heterocyclic compounds. These findings highlight the competitive predictive ability of the SCQM model as compared to other models across analogous datasets. With an R2 value close to 1 and a very low RMSE value, the SCQM model emerged as a reliable predictor of the properties of N-heterocyclic compounds. This underlines the significant potential of the SCQM approach in understanding and predicting the intricate chemical properties of complex compounds like N-heterocycles.

3.3. *Quantum information analysis*

Classical models face limitations in accessing quantum information due to the intricacies of quantum mechanics, including superposition and entanglement. Quantum particles in superposition can exist in multiple states simultaneously, posing challenges for classical representation. Quantum algorithms exploit this simultaneous representation, computing all possibilities simultaneously, unlike classical models that evaluate one state at a time. Even over large distances, the entanglement of quantum particles presents complex, non-local dependencies that are challenging for classical models. Heisenberg's uncertainty principle further complicates obtaining precise information through classical measurements. Quantum phenomena, primarily those closely tied to particle or system properties, provide intricate information beyond classical models' reach. While classical models handle basic quantum features, they may struggle with the subtleties of complex quantum properties. Quantum algorithms, designed to leverage these properties, excel in performing rigorous computations in specific scenarios, such as the results of DFT calculations.

This case study shows that SCQM consistently exhibits superior prediction performance compared to classical models, as shown in Table 4 and Fig. 6. Further analysis through Fig. 7, which compares the feature importance and Shapley additive explanations (SHAP) values between SCQM and classical models such as RF, highlights the important role of QNN in this hybrid framework. RF is chosen as a representative classical model for feature importance (Fig. 7) and SHAP values (Fig. 8) analysis. Fig. 7 demonstrates that SCQM produces higher overall feature importance values than RF, with total importance values of 1.37 and 0.59, respectively. This significant difference indicates that SCQM assigns a greater weight to quantum-based features, emphasizing its ability to exploit these attributes for superior prediction accuracy. Features such as polarizability (σ) and electrophilicity index (ω), which are highly relevant in understanding the inhibitor's properties, show markedly higher importance in SCQM, highlighting the effectiveness of QNN in capturing relevant patterns that classical models might overlook. SHAP analysis, presented in Fig. 8, provides additional depth in understanding how each feature contributes to the model output (Prendin et al., 2023), (Mangalathu et al., 2020), (Nohara et al., 2022).

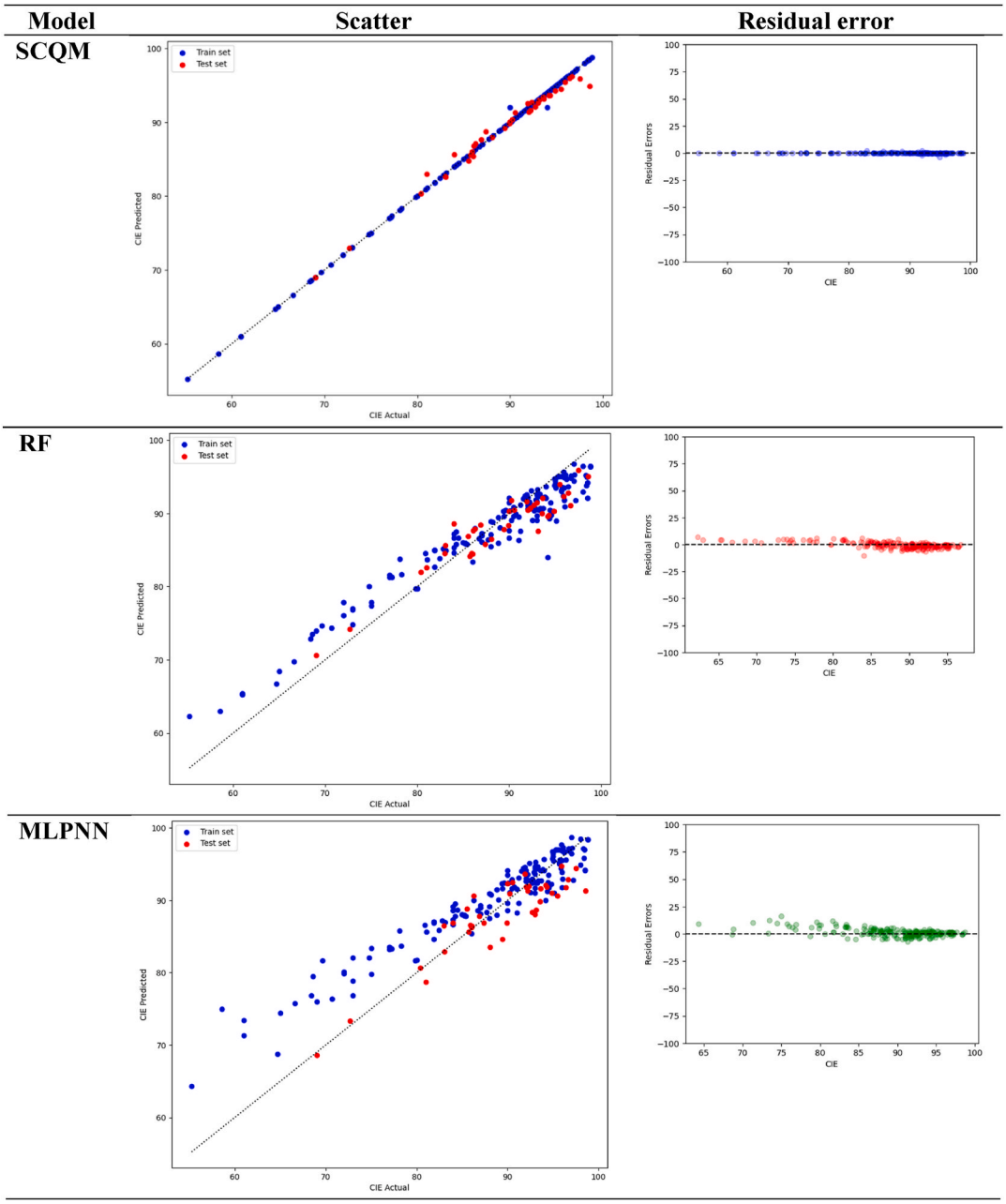

Fig. 6. Scatter and residual error plot of data point prediction by models.

Table 5
Predictive performance of models for derivatives N-heterocycles datasets.

Dataset	Samples	Model	R^2	RMSE	Ref.
Pyridazine	20	ANN	–	10.56	Quadri et al. (2022b)
Pyridazine	21	ANN	0.90	–	El Assiri et al. (2020b)
Pyrimidine	40	ANN	–	2.91	Quadri et al. (2022c)
Pyrimidine	54	RF	–	5.71	Alamri and Alhazmi (2022)
Pyridine-quinoline	41	GA-ANN	–	16.74	Ser et al. (2020b)
Pyridine-quinoline	28	MLR	0.93	–	Camacho-Mendoza et al. (2022)
Quinoxaline	40	MLPNN	–	5.42	Quadri et al. (2022d)
N-heterocycles	195	SCQM	0.98	0.92	This work

For SCQM, the SHAP values exhibit a tighter and more pronounced concentration than RF, suggesting that the hybrid model captures the contribution of features with higher precision and consistency. Key quantum descriptors like electronegativity (χ) and dipole moment (μ) demonstrate broader SHAP value distributions in RF, indicating more significant uncertainty and inconsistency in feature contributions. Conversely, SCQM shows more focused and stable distributions for these features, indicating its advantage in modeling non-linear interactions

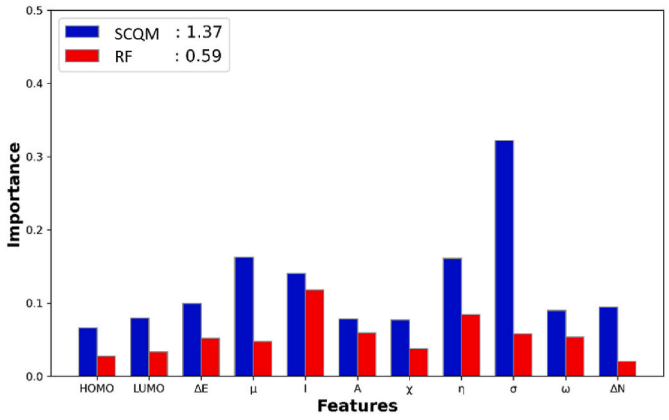

Fig. 7. Comparison of feature importance from models.

intrinsic to quantum data. A noteworthy observation in SHAP patterns is the distinct ability of SCQM to capture the synergistic effects of features. For example, the combined impact of global electrophilicity index (ω) and electronic chemical potential (η) is represented in SCQM's SHAP values but remains fragmented in RF. This finding supports the hypothesis that QNN's representational power allows for deeper insights into the relationship between quantum descriptors and corrosion inhibition efficiency, effectively outperforming RF. Integrating QNN in the hybrid stacking framework enhances the model's capacity to handle and interpret quantum features, enabling superior performance in tasks requiring analysis of non-linear, complex data relationships. As demonstrated, the use of SHAP analysis verifies the effectiveness of SCQM. It provides a pathway to understanding its inner workings, paving the way for developing more advanced hybrid quantum-classical systems.

3.4. Model application

Lachhab et al. (2024) recently conducted an assessment using experimental approaches to determine the corrosion inhibition potential of novel N-heterocyclic derivative compounds, specifically, N-((3, 5-dimethyl-1H-pyrazol-1-yl)methyl)pyrimidine-2-amine (PP1) and ethyl-5-methyl-1-((pyrimidin-2-yl-amino)methyl) 1H-pyrazole-3-carboxylate (PP2). The outcomes unveiled the CIE values of approximately 91.15 and 92.39 for PP1 and PP2, respectively. Our study focuses on forecasting the CIE values of these chemical entities utilizing the validated SCQM approach. As per the prognostic outcomes detailed in Table 6, both compounds yield CIE values of 90.87 and 91.96, respectively. These projections authenticate the credibility of our proposed methodology as a reliable technique. Moreover, these predictions align with the observed trends and mirror the values derived from experimental assessments. The estimated CIE values highlighted in Table 6 underscore the potential of these newly synthesized inhibitor

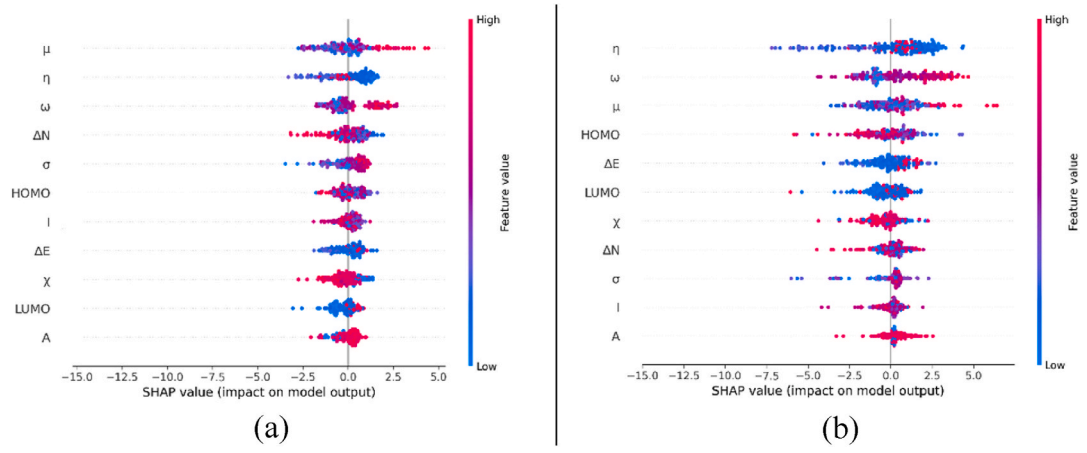

Fig. 8. SHAP plot between (a) SCQM and (b) RF models.

Table 6
The CIE of novel N-heterocycles-derived compounds.

Inhibitor	Structure	CIE (%)			
		SCQM	**MLPNN**	**RF**	**Exp.** (Lachhab et al., 2024)
PP1	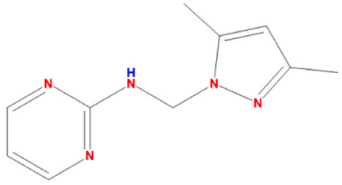	90.87	88.75	89.31	91.15
PP2	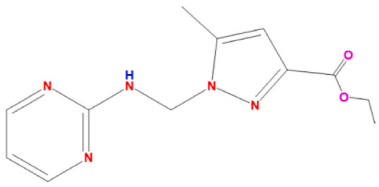	91.96	89.82	90.33	92.39

compounds to offer protective capabilities. These outcomes signify the potential efficacy of these substances as highly potent corrosion inhibitors.

4. Conclusion

This study demonstrates the significant benefits of QNN in the stacking classical-quantum model framework for predicting the CIE of N-heterocyclic compounds. With superior performance metrics, R^2 of 0.98, RMSE of 0.92, MSE of 0.64, MAD of 0.52, and MAPE of 0.71, SCQM shows clear superiority over classical models such as MLPNN and RF. The model's accuracy is reflected in the prediction of new N-heterocyclic derivatives, N-((3,5-dimethyl-1H-pyrazol-1-yl)methyl)pyrimidine-2-amine (PP1) and ethyl-5-methyl-1-((pyrimidin-2-yl-amino)methyl) 1H-pyrazole-3-carboxylate (PP2), with CIE values of 95.39% and 94.05%, respectively, confirming the ability of SCQM to produce accurate and reliable predictions. The presence of QNN in the SCQM framework is crucial, especially in its ability to capture and utilize complex quantum information that is difficult to handle by classical models. Statistical analysis shows that the features based on the quantum principle of QCP contribute significantly to the CIE values and have a high correlation with them. This underlines the power of SCQM in integrating the advantages of classical and quantum models to produce superior predictions. This study demonstrates the potential of SCQM in anti-corrosion material exploration and provides a foundation for further development in anti-corrosion property prediction utilizing quantum methods. To improve the generalization of predictions, future studies are suggested to expand the scope of the dataset by involving more types of compounds. Thus, this study becomes an important stepping stone to encourage the utilization of quantum models in artificial intelligence-based material innovation.

CRediT authorship contribution statement

Muhamad Akrom: Writing – original draft, Methodology, Investigation, Formal analysis, Data curation, Conceptualization. **Supriadi Rustad:** Writing – original draft, Supervision, Methodology, Formal analysis, Conceptualization. **Totok Sutojo:** Methodology, Conceptualization. **Wahyu Aji Eko Prabowo:** Investigation, Formal analysis. **Hermawan Kresno Dipojono:** Supervision, Methodology, Conceptualization. **Ryo Maezono:** Supervision. **Hideaki Kasai:** Supervision.

Declaration of competing interest

The author declares that they have no known competing financial or non-financial interests or personal relationships that could have appeared to influence the work reported in this paper.

Acknowledgments

All calculations were performed using the Computation Facility at the Research Center for Quantum Computing and Materials Informatics, Universitas Dian Nuswantoro and IBM Quantum Learning. MA acknowledges BRIN-LPDP support for RIIM-G7 program in 2025.

Data availability

Data will be made available on request.

References

Abban, O.J., et al., 2023. Policies for carbon-zero targets: examining the spillover effects of renewable energy and patent applications on environmental quality in Europe. Energy Econ. 126, 106954. https://doi.org/10.1016/J.ENECO.2023.106954.

Abbas, A., Sutter, D., Zoufal, C., Lucchi, A., Figalli, A., Woerner, S., 2021. The power of quantum neural networks. Nat Comput Sci 1 (6), 403–409. https://doi.org/10.1038/s43588-021-00084-1.

Abdulsalam, G., Meshoul, S., Shaiba, H., 2023. Explainable heart disease prediction using ensemble-quantum machine learning approach. Intelligent Automation and Soft Computing 36 (1), 761–779. https://doi.org/10.32604/iasc.2023.032262.

Agrawal, A., Choudhary, A., 2019. Deep Materials Informatics: Applications of Deep Learning in Materials Science. Cambridge University Press. https://doi.org/10.1557/mrc.2019.73.

Ahsan, M., Mahmud, M., Saha, P., Gupta, K., Siddique, Z., 2021. Effect of data scaling methods on machine learning algorithms and model performance. Technologies 9 (3), 52. https://doi.org/10.3390/technologies9030052.

Aishwarya, S., Abeer, V., Sathish, B.B., Subramanya, K.N., 2020. Quantum computational techniques for prediction of cognitive state of human mind from EEG signals. Journal of Quantum Computing 2 (4), 157–170. https://doi.org/10.32604/jqc.2020.015018.

Akrom, M., 2024a. Green corrosion inhibitors for iron alloys: a comprehensive review of integrating data-driven forecasting, density functional theory simulations, and experimental investigation. Journal of Multiscale Materials Informatics 1 (1), 22–37. https://doi.org/10.62411/jimat.v1i1.10495.

Akrom, M., 2024b. Quantum support vector machine for classification task: a review. Journal of Multiscale Materials Informatics 1 (2), 1–8. https://doi.org/10.62411/jimat.v1i2.10965.

Akrom, M., Rustad, S., Kresno Dipojono, H., 2023a. Machine learning investigation to predict corrosion inhibition capacity of new amino acid compounds as corrosion inhibitors. Results Chem, 101126. https://doi.org/10.1016/J.RECHEM.2023.101126.

Akrom, M., Sutojo, T., Pertiwi, A., Rustad, S., Kresno Dipojono, H., 2023b. Investigation of best QSPR-based machine learning model to predict corrosion inhibition performance of pyridine-quinoline compounds. J Phys Conf Ser 2673 (1), 012014. https://doi.org/10.1088/1742-6596/2673/1/012014.

Akrom, M., Rustad, S., Saputro, A.G., Dipojono, H.K., 2023c. Data-driven investigation to model the corrosion inhibition efficiency of Pyrimidine-Pyrazole hybrid corrosion inhibitors. Comput Theor Chem 1229, 114307. https://doi.org/10.1016/J.COMPTC.2023.114307.

Akrom, M., et al., 2023d. DFT and microkinetic investigation of oxygen reduction reaction on corrosion inhibition mechanism of iron surface by Syzygium Aromaticum extract. Appl. Surf. Sci. 615 (Apr). https://doi.org/10.1016/j.apsusc.2022.156319.

Akrom, M., Rustad, S., Saputro, A.G., Ramelan, A., Fathurrahman, F., Dipojono, H.K., 2023e. A combination of machine learning model and density functional theory method to predict corrosion inhibition performance of new diazine derivative compounds. Mater. Today Commun. 35, 106402. https://doi.org/10.1016/J.MTCOMM.2023.106402.

Akrom, M., Rustad, S., Dipojono, H.K., 2024a. A machine learning approach to predict the efficiency of corrosion inhibition by natural product-based organic inhibitors. Phys. Scri. 99 (3), 036006. https://doi.org/10.1088/1402-4896/ad28a9.

Akrom, M., Rustad, S., Kresno Dipojono, H., 2024b. Prediction of Anti-Corrosion performance of new triazole derivatives via Machine learning. Comput Theor Chem 1236 (Jun). https://doi.org/10.1016/j.comptc.2024.114599.

Akrom, M., Rustad, S., Dipojono, H.K., 2024c. Investigation of corrosion inhibition capability of pyridazine compounds via ensemble learning. J. Mater. Eng. Perform. https://doi.org/10.1007/s11665-024-10129-x.

Akrom, M., Rustad, S., Dipojono, H.K., 2024d. Variational quantum circuit-based quantum machine learning approach for predicting corrosion inhibition efficiency of pyridine-quinoline compounds. Materials Today Quantum 2, 100007. https://doi.org/10.1016/j.mtquan.2024.100007.

Akrom, M., Rustad, S., Dipojono, H.K., 2024e. Development of quantum machine learning to evaluate the corrosion inhibition capability of pyrimidine compounds. Mater. Today Commun., 108758 https://doi.org/10.1016/J.MTCOMM.2024.108758.

Akrom, M., Rustad, S., Dipojono, H.K., 2024f. SMILES-based machine learning enables the prediction of corrosion inhibition capacity. MRS Commun. https://doi.org/10.1557/s43579-024-00551-6.

Akrom, M., Rustad, S., Dipojono, H.K., Maezono, R., Kasai, H., 2025. Quantum machine learning for ABO3 perovskite structure prediction. Comput. Mater. Sci. 250, 113694. https://doi.org/10.1016/j.commatsci.2025.113694.

Al Azies, H., Akrom, M., Rustad, S., Dipojono, H.K., 2024. Robust machine learning for predicting thermal stability of metal-organic framework. Chemistry Africa. https://doi.org/10.1007/s42250-024-01080-4.

Alamri, A.H., Alhazmi, N., 2022. Development of data driven machine learning models for the prediction and design of pyrimidine corrosion inhibitors. J. Saudi Chem. Soc. 26 (6). https://doi.org/10.1016/j.jscs.2022.101536.

Alcazar, J., Leyton-Ortega, V., Perdomo-Ortiz, A., 2020. Classical versus quantum models in machine learning: insights from a finance application. Mach Learn Sci Technol 1 (3). https://doi.org/10.1088/2632-2153/AB9009.

Alhayani, B.A., AlKawak, O.A., Mahajan, H.B., Ilhan, H., Qasem, R.M., 2023. Design of Quantum Communication Protocols in Quantum Cryptography. Wirel Pers Commun. https://doi.org/10.1007/s11277-023-10587-x.

Alsubai, S., Alqahtani, A., Binbusayyis, A., Sha, M., Gumaei, A., Wang, S., 2023. Heart failure detection using instance quantum circuit approach and traditional predictive analysis. Mathematics 11 (6). https://doi.org/10.3390/math11061467.

Arrousse, N., et al., 2020. The inhibition behavior of two pyrimidine-pyrazole derivatives against corrosion in hydrochloric solution: experimental, surface analysis and in silico approach studies. Arab. J. Chem. 13 (7), 5949–5965. https://doi.org/10.1016/j.arabjc.2020.04.030.

S. Bafandeh, I. And, and M. Bolandraftar, "Application of K-Nearest Neighbor (KNN) Approach for Predicting Economic Events: Theoretical Background."[Online]. Available: www.ijera.com.

Belghiti, M.E., et al., 2019. Computational simulation and statistical analysis on the relationship between corrosion inhibition efficiency and molecular structure of some hydrazine derivatives in phosphoric acid on mild steel surface. Appl. Surf. Sci. 491, 707–722. https://doi.org/10.1016/J.APSUSC.2019.04.125.

Beltran-Perez, C., et al., 2022. A general use QSAR-ARX model to predict the corrosion inhibition efficiency of drugs in terms of quantum mechanical descriptors and experimental comparison for lidocaine. Int. J. Mol. Sci. 23 (9). https://doi.org/10.3390/ijms23095086.

Ben Seghier, M.E.A., Höche, D., Zheludkevich, M., 2022. Prediction of the internal corrosion rate for oil and gas pipeline: implementation of ensemble learning techniques. J. Nat. Gas Sci. Eng. 99 (Mar). https://doi.org/10.1016/j.jngse.2022.104425.

Benedetti, M., Lloyd, E., Sack, S., Fiorentini, M., 2019. "Erratum: parameterized quantum circuits as machine learning models. Quantum Sci. Technol. 4, 043001. https://doi.org/10.1088/2058-9565/ab5944, 10.1088/2058-9565/ab4eb5)," 2020, Institute of Physics Publishing.

Beniken, M., et al., 2023. Electrochemistry evaluation and quantum corroboration with surface analysis of potential anticorrosive of two new pyridazine derivatives for mild steel in 1 M HCl solution. Colloids Surf. A Physicochem. Eng. Asp. 673 (Sep). https://doi.org/10.1016/j.colsurfa.2023.131699.

Biamonte, J., Wittek, P., Pancotti, N., Rebentrost, P., Wiebe, N., Lloyd, S., 2017a. Quantum Machine Learning. Nature Publishing Group. https://doi.org/10.1038/nature23474.

Biamonte, J., Wittek, P., Pancotti, N., Rebentrost, P., Wiebe, N., Lloyd, S., 2017b. Quantum Machine Learning. Nature Publishing Group. https://doi.org/10.1038/nature23474.

Botchkarev, A., 2019. A new typology design of performance metrics to measure errors in machine learning regression algorithms. Interdiscipl. J. Inf. Knowl. Manag. 14, 45–76. https://doi.org/10.28945/4184.

Brown, P., Zhuang, H., 2023. Quantum machine-learning phase prediction of high-entropy alloys. Mater. Today 63, 18–31. https://doi.org/10.1016/j.mattod.2023.02.014.

Budi, S., et al., 2024. Implementation of polynomial functions to improve the accuracy of machine learning models in predicting the corrosion inhibition efficiency of pyridine-quinoline compounds as corrosion inhibitors. KnE Engineering. https://doi.org/10.18502/keg.v6i1.15351.

Calafat-Marzal, C., Sánchez-García, M., Gallego-Salguero, A., Piñeiro, V., 2023. Drivers of winegrowers' decision on land use abandonment based on exploratory spatial data analysis and multilevel models. Land Use Policy 132, 106807. https://doi.org/10.1016/J.LANDUSEPOL.2023.106807.

Camacho-Mendoza, R.L., Feria, L., Zárate-Hernández, L.Á., Alvarado-Rodríguez, J.G., Cruz-Borbolla, J., 2022. New QSPR model for prediction of corrosion inhibition using conceptual density functional theory. J. Mol. Model. 28 (8). https://doi.org/10.1007/s00894-022-05240-6.

Chauhan, D.S., Singh, P., Quraishi, M.A., 2020. Quinoxaline derivatives as efficient corrosion inhibitors: current status, challenges and future perspectives. J. Mol. Liq. 320, 114387. https://doi.org/10.1016/J.MOLLIQ.2020.114387.

Ciliberto, C., et al., 2018. Quantum Machine Learning: A Classical Perspective. Royal Society Publishing. https://doi.org/10.1098/rspa.2017.0551.

Cong, I., Choi, S., Lukin, M.D., 2019. Quantum convolutional neural networks. Nat. Phys. 15 (12), 1273–1278. https://doi.org/10.1038/s41567-019-0648-8.

Cui, Y., Zhang, T., Wang, F., 2022. New understanding on the mechanism of organic inhibitors for magnesium alloy. Corros. Sci. 198, 110118. https://doi.org/10.1016/J.CORSCI.2022.110118.

Deng, Z., Wang, X., Dong, B., 2023. Quantum computing for future real-time building HVAC controls. Appl. Energy 334, 120621. https://doi.org/10.1016/J.APENERGY.2022.120621.

Echihi, S., et al., 2023. Experimental and theoretical investigation to the mild steel's corrosion inhibition using pyrazole pyrimidine derivative. Chemical Data Collections 46, 101049. https://doi.org/10.1016/j.cdc.2023.101049.

El Assiri, E.H., et al., 2020a. Development and validation of QSPR models for corrosion inhibition of carbon steel by some pyridazine derivatives in acidic medium. Heliyon 6 (10), e05067. https://doi.org/10.1016/j.heliyon.2020.e05067.

El Assiri, E.H., et al., 2020b. Development and validation of QSPR models for corrosion inhibition of carbon steel by some pyridazine derivatives in acidic medium. Heliyon 6 (10), e05067. https://doi.org/10.1016/j.heliyon.2020.e05067.

Elsedimy, E.I., AboHashish, S.M.M., Algarni, F., 2023. New cardiovascular disease prediction approach using support vector machine and quantum-behaved particle swarm optimization. Multimed. Tool. Appl. https://doi.org/10.1007/s11042-023-16194-z.

Erdoğan, Ş., Safi, Z.S., Kaya, S., Işın, D.Ö., Guo, L., Kaya, C., 2017. A computational study on corrosion inhibition performances of novel quinoline derivatives against the corrosion of iron. J. Mol. Struct. 1134, 751–761. https://doi.org/10.1016/J.MOLSTRUC.2017.01.037.

Ghazoui, A., et al., 2013. An investigation of two novel pyridazine derivatives as corrosion inhibitor for C38 steel in 1.0 M HCl. Int. J. Electrochem. Sci. 8 (2), 2272–2292. https://doi.org/10.1016/S1452-3981(23)14308-2.

Grant, E., et al., 2018. Hierarchical quantum classifiers. npj Quantum Inf 4 (1). https://doi.org/10.1038/s41534-018-0116-9.

Gupta, H., Varshney, H., Sharma, T.K., Pachauri, N., Verma, O.P., 2022. Comparative performance analysis of quantum machine learning with deep learning for diabetes prediction. Complex and Intelligent Systems 8 (4), 3073–3087. https://doi.org/10.1007/s40747-021-00398-7.

Havlíček, V., et al., 2019. Supervised learning with quantum-enhanced feature spaces. Nature 567 (7747), 209–212. https://doi.org/10.1038/s41586-019-0980-2.

Herowati, W., et al., 2024a. Prediction of corrosion inhibition efficiency based on machine learning for pyrimidine compounds: a comparative study of linear and non-linear algorithms. KnE Engineering. https://doi.org/10.18502/keg.v6i1.15350.

Herowati, W., et al., 2024b. Machine learning for pyrimidine corrosion inhibitor small dataset. Theor. Chem. Acc. 143 (8). https://doi.org/10.1007/s00214-024-03140-x.

Ibarra-Vazquez, G., Ramírez-Montoya, M.S., Miranda, J., 2023. Data analysis in factors of social entrepreneurship tools in complex thinking: an exploratory study. Think. Skills Creativ. 49, 101381. https://doi.org/10.1016/J.TSC.2023.101381.

Imanothai, T., Taetragool, U., 2023. The Effects of Training Quantum Support Vector Machines with Different Samples from the Same Dataset, 070006. https://doi.org/10.1063/5.0178310.

Jiang, L., Qiang, Y., Lei, Z., Wang, J., Qin, Z., Xiang, B., 2018. Excellent corrosion inhibition performance of novel quinoline derivatives on mild steel in HCl media: experimental and computational investigations. J. Mol. Liq. 255, 53–63. https://doi.org/10.1016/J.MOLLIQ.2018.01.133.

Jin, H., Blackwood, D.J., Wang, Y., Ng, M.F., Tan, T.L., 2022. First-principles study of surface orientation dependent corrosion of BCC iron. Corros. Sci. 196, 110029. https://doi.org/10.1016/J.CORSCI.2021.110029.

Kavitha, S.S., Kaulgud, N., 2023. Quantum K-means clustering method for detecting heart disease using quantum circuit approach. Soft Comput. 27 (18), 13255–13268. https://doi.org/10.1007/s00500-022-07200-x.

Kholili, M.J., Muslim, R., Nugraha, A.R.T., 2023. A Classical Algorithm Inspired by Quantum Neural Network for Solving a Bose-Hubbard-like System in Phase-Space Representation, 070007. https://doi.org/10.1063/5.0178381.

Khoutoul, M., et al., 2014. Theoretical approach to the corrosion inhibition efficiency of some pyrimidine derivatives using DFT method of mild steel in HCl solution. Available online www.jocpr.com Journal of Chemical and Pharmaceutical Research 6 (4), 1216–1224 [Online]. Available: http://www.jmaterenvironsci.com.

Kozlica, D.K., Kokalj, A., Milošev, I., 2021. Synergistic effect of 2-mercaptobenzimidazole and octylphosphonic acid as corrosion inhibitors for copper and aluminium – an electrochemical, XPS, FTIR and DFT study. Corros. Sci. 182, 109082. https://doi.org/10.1016/J.CORSCI.2020.109082.

Kumar, D., Jain, V., Rai, B., 2022a. Capturing the synergistic effects between corrosion inhibitor molecules using density functional theory and ReaxFF simulations - a case for benzyl azide and butyn-1-ol on Cu surface. Corros. Sci. 195 (Feb). https://doi.org/10.1016/j.corsci.2021.109960.

Kumar, D., Jain, V., Rai, B., 2022b. Capturing the synergistic effects between corrosion inhibitor molecules using density functional theory and ReaxFF simulations - a case for benzyl azide and butyn-1-ol on Cu surface. Corros. Sci. 195 (Feb). https://doi.org/10.1016/j.corsci.2021.109960.

Kwak, Y., Yun, W.J., Jung, S., Kim, J., 2021a. Quantum neural networks: concepts, applications, and challenges [Online]. Available: http://arxiv.org/abs/2108.01468.

Kwak, Y., Yun, W.J., Jung, S., Kim, J., 2021b. Quantum neural networks: concepts, applications, and challenges [Online]. Available: http://arxiv.org/abs/2108.01468.

Lachhab, H., et al., 2024. Detailed experimental performance of two new pyrimidine-pyrazole derivatives as corrosion inhibitors for mild steel in HCl media combined with DFT/MDs simulations of bond breaking upon adsorption. Colloids Surf. A Physicochem. Eng. Asp. 680, 132649. https://doi.org/10.1016/j.colsurfa.2023.132649.

Lim, S., Chi, S., 2019. Xgboost application on bridge management systems for proactive damage estimation. Adv. Eng. Inform. 41 (Aug). https://doi.org/10.1016/j.aei.2019.100922.

Linden, J., Marquis, R., 2023. The influence of time on dynamic signature: an exploratory data analysis. Forensic Sci. Int. 348, 111577. https://doi.org/10.1016/J.FORSCIINT.2023.111577.

Liu, Y., et al., 2019. A machine learning-based QSAR model for benzimidazole derivatives as corrosion inhibitors by incorporating comprehensive feature selection. Interdiscip Sci 11 (4), 738–747. https://doi.org/10.1007/s12539-019-00346-7.

Luo, W., et al., 2021. A new pyridazine derivative synthesized as an efficient corrosion inhibitor for copper in sulfuric acid medium: experimental and theoretical calculation studies. J. Mol. Liq. 341, 117370. https://doi.org/10.1016/J.MOLLIQ.2021.117370.

Ma, H., Liu, J., Shang, H., Fan, Y., Li, Z., Yang, J., 2023. Multiscale quantum algorithms for quantum chemistry. Chem. Sci. 14 (12), 3190–3205. https://doi.org/10.1039/d2sc06875c.

Mangalathu, S., Hwang, S.H., Jeon, J.S., 2020. Failure mode and effects analysis of RC members based on machine-learning-based SHapley Additive exPlanations (SHAP) approach. Eng. Struct. 219, 110927. https://doi.org/10.1016/J.ENGSTRUCT.2020.110927.

Masuku, G.M., Nxumalo, W., Kabanda, M.M., Murulana, L.C., Bahadur, I., 2023. Quinoxaline derivatives as corrosion inhibitors of zinc in 1.0 M hydrochloric and sulphuric acid solutions: adsorption, electrochemical, spectroscopic, and computational studies. J. Mol. Liq., 122458 https://doi.org/10.1016/j.molliq.2023.122458.

Mehdi, M., Zandi, S., 2019. Computational Evaluation of Corrosion Inhibition of Four Quinoline Derivatives on Carbon Steel in Aqueous Phase.

Mishra, N., et al., 2021. Quantum machine learning: a review and current status. In: Advances in Intelligent Systems and Computing. Springer Science and Business Media Deutschland GmbH, pp. 101–145. https://doi.org/10.1007/978-981-15-5619-7_8.

Mitarai, K., Negoro, M., Kitagawa, M., Fujii, K., 2018. Quantum circuit learning. Phys Rev A (Coll Park) 98 (3). https://doi.org/10.1103/PhysRevA.98.032309.

Mrani, S.A., et al., 2023. Experimental, theoretical and MC simulation investigations of the inhibitory efficiency of novel non-toxic pyridazine derivatives inhibition on

carbon steel in 1 M HCl solution. J. Mol. Liq. 382 (Jul). https://doi.org/10.1016/j.molliq.2023.122043.
Narain, R., Saxena, S., Goyal, A.K., 2016. Cardiovascular risk prediction: a comparative study of framingham and quantum neural network based approach. Patient Prefer. Adherence 10, 1259–1270. https://doi.org/10.2147/PPA.S108203.
Nohara, Y., Matsumoto, K., Soejima, H., Nakashima, N., 2022. Explanation of machine learning models using shapley additive explanation and application for real data in hospital. Comput. Methods Progr. Biomed. 214, 106584. https://doi.org/10.1016/J.CMPB.2021.106584.
Obot, I.B., Umoren, S.A., 2020. Experimental, DFT and QSAR models for the discovery of new pyrazines corrosion inhibitors for steel in oilfield acidizing environment. Int. J. Electrochem. Sci. 15 (9), 9066–9080. https://doi.org/10.20964/2020.09.72.
Ozpolat, Z., Karabatak, M., 2023. Performance evaluation of quantum-based machine learning algorithms for cardiac arrhythmia classification. Diagnostics 13 (6). https://doi.org/10.3390/diagnostics13061099.
Pately, P.D., Pately, M.R., Kaushik-Basu, N., Talele, T.T., 2008. 3D QSAR and molecular docking studies of benzimidazole derivatives as hepatitis C virus NS5B polymerase inhibitors. J. Chem. Inf. Model. 48 (1), 42–55. https://doi.org/10.1021/ci700266z.
Prendin, F., Pavan, J., Cappon, G., Del Favero, S., Sparacino, G., Facchinetti, A., 2023. The importance of interpreting machine learning models for blood glucose prediction in diabetes: an analysis using SHAP. Sci. Rep. 13 (1). https://doi.org/10.1038/s41598-023-44155-x.
Putra, R.I.D., Maulana, A.L., Saputro, A.G., 2019. Study on building machine learning model to predict biodegradable-ready materials. In: AIP Conference Proceedings. American Institute of Physics Inc. https://doi.org/10.1063/1.5095351
Pyrkov, A., et al., 2023. Quantum computing for near-term applications in generative chemistry and drug discovery. Drug Discov. Today 28 (8), 103675. https://doi.org/10.1016/J.DRUDIS.2023.103675.
Qi, J., Yang, C.H.H., Chen, P.Y., Hsieh, M.H., 2023. Theoretical error performance analysis for variational quantum circuit based functional regression. npj Quantum Inf 9 (1). https://doi.org/10.1038/s41534-022-00672-7.
Quadri, T.W., et al., 2022a. Multilayer perceptron neural network-based QSAR models for the assessment and prediction of corrosion inhibition performances of ionic liquids. Comput. Mater. Sci. 214 (Nov). https://doi.org/10.1016/j.commatsci.2022.111753.
Quadri, T.W., et al., 2022b. Development of QSAR-based (MLR/ANN) predictive models for effective design of pyridazine corrosion inhibitors. Mater. Today Commun. 30 (Mar). https://doi.org/10.1016/j.mtcomm.2022.103163.
Quadri, T.W., et al., 2022c. Predicting protection capacities of pyrimidine-based corrosion inhibitors for mild steel/HCl interface using linear and nonlinear QSPR models. J. Mol. Model. 28 (9). https://doi.org/10.1007/s00894-022-05245-1.
Quadri, T.W., et al., 2022d. Computational insights into quinoxaline-based corrosion inhibitors of steel in HCl: quantum chemical analysis and QSPR-ANN studies. Arab. J. Chem. 15 (7). https://doi.org/10.1016/j.arabjc.2022.103870.
Rasheeda, K., Alva, V.D.P., Krishnaprasad, P.A., Samshuddin, S., 2018. Pyrimidine derivatives as potential corrosion inhibitors for steel in acid medium – an overview. International Journal of Corrosion and Scale Inhibition 7 (1), 48–61. https://doi.org/10.17675/2305-6894-2018-7-1-5.
Rosyid, M.R., Mawaddah, L., Santosa, A.P., Akrom, M., Rustad, S., Dipojono, H.K., 2024. Implementation of quantum machine learning in predicting corrosion inhibition efficiency of expired drugs. Mater. Today Commun. 40, 109830. https://doi.org/10.1016/J.MTCOMM.2024.109830.
Rustad, S., Akrom, M., Sutojo, T., Dipojono, H.K., 2024. A feature restoration for machine learning on anti-corrosion materials. Case Studies in Chemical and Environmental Engineering 10, 100902. https://doi.org/10.1016/J.CSCEE.2024.100902.
Sagingalieva, A., Kordzanganeh, M., Kenbayev, N., Kosichkina, D., Tomashuk, T., Melnikov, A., 2023. Hybrid quantum neural network for drug response prediction. Cancers 15 (10). https://doi.org/10.3390/cancers15102705.
Saranya, J., Sowmiya, M., Sounthari, P., Parameswari, K., Chitra, S., Senthilkumar, K., 2016. N-heterocycles as corrosion inhibitors for mild steel in acid medium. J. Mol. Liq. 216, 42–52. https://doi.org/10.1016/J.MOLLIQ.2015.12.096.
Sarkar, T.K., Saraswat, V., Mitra, R.K., Obot, I.B., Yadav, M., 2021. Mitigation of corrosion in petroleum oil well/tubing steel using pyrimidines as efficient corrosion inhibitor: experimental and theoretical investigation. Mater. Today Commun. 26, 101862. https://doi.org/10.1016/J.MTCOMM.2020.101862.
Sayed, G.H., Azab, M.E., Anwer, K.E., Raouf, M.A., Negm, N.A., 2018. Pyrazole, pyrazolone and enaminonitrile pyrazole derivatives: synthesis, characterization and potential in corrosion inhibition and antimicrobial applications. J. Mol. Liq. 252, 329–338. https://doi.org/10.1016/J.MOLLIQ.2017.12.156.
Schuld, M., Killoran, N., 2019. Quantum machine learning in feature Hilbert spaces. Phys. Rev. Lett. 122 (4). https://doi.org/10.1103/PhysRevLett.122.040504.
Schuld, M., Bocharov, A., Svore, K.M., Wiebe, N., 2020. Circuit-centric quantum classifiers. Phys Rev A (Coll Park) 101 (3). https://doi.org/10.1103/PhysRevA.101.032308.
Ser, C.T., Žuvela, P., Wong, M.W., 2020a. Prediction of corrosion inhibition efficiency of pyridines and quinolines on an iron surface using machine learning-powered quantitative structure-property relationships. Appl. Surf. Sci. 512. https://doi.org/10.1016/j.apsusc.2020.145612.
Ser, C.T., Žuvela, P., Wong, M.W., 2020b. Prediction of corrosion inhibition efficiency of pyridines and quinolines on an iron surface using machine learning-powered quantitative structure-property relationships. Appl. Surf. Sci. 512. https://doi.org/10.1016/j.apsusc.2020.145612.
Sutojo, T., Rustad, S., Akrom, M., Syukur, A., Shidik, G.F., Dipojono, H.K., 2023. A machine learning approach for corrosion small datasets. npj Mater. Degrad. 7 (1). https://doi.org/10.1038/s41529-023-00336-7.
Suzuki, T., Katouda, M., 2020. Predicting toxicity by quantum machine learning. J Phys Commun 4 (12). https://doi.org/10.1088/2399-6528/abd3d8.
Toropov, A.A., Toropova, A.P., 2020. QSPR/QSAR: State-Of-Art,weirdness, the Future. MDPI AG. https://doi.org/10.3390/molecules25061292.
Trisnapradika, G.A., Akrom, M., Rustad, S., Dipojono, H.K., Maezono, R., Kasai, H., 2025. A machine learning approach for forecasting the efficacy of pyridazine corrosion inhibitors. Theor. Chem. Acc. 144 (1). https://doi.org/10.1007/s00214-024-03165-2.
Verma, C.B., Ebenso, E.E., Bahadur, I., Obot, I.B., Quraishi, M.A., 2015. 5-(Phenylthio)-3H-pyrrole-4-carbonitriles as effective corrosion inhibitors for mild steel in 1 M HCl: experimental and theoretical investigation. J. Mol. Liq. 212, 209–218. https://doi.org/10.1016/J.MOLLIQ.2015.09.009.
Verma, C., Rhee, K.Y., Quraishi, M.A., Ebenso, E.E., 2020. Pyridine based N-heterocyclic compounds as aqueous phase corrosion inhibitors: a review. J. Taiwan Inst. Chem. Eng. 117, 265–277. https://doi.org/10.1016/J.JTICE.2020.12.011.
Verma, C., Abdellattif, M.H., Alfantazi, A., Quraishi, M.A., 2021. N-heterocycle compounds as aqueous phase corrosion inhibitors: a robust, effective and economic substitute. J. Mol. Liq. 340, 117211. https://doi.org/10.1016/J.MOLLIQ.2021.117211.
Wieder, M., Fass, J., Chodera, J.D., 2021. Fitting quantum machine learning potentials to experimental free energy data: predicting tautomer ratios in solution. Chem. Sci. 12 (34), 11364–11381. https://doi.org/10.1039/d1sc01185e.
Xia, R., Kais, S., 2019. Hybrid Quantum-Classical Neural Network for Calculating Ground State Energies of Molecules. https://doi.org/10.3390/e22080828.
Yuan, X., Ge, Z., Song, Z., 2014. Soft sensor model development in multiphase/multimode processes based on Gaussian mixture regression. Chemometr. Intell. Lab. Syst. 138, 97–109. https://doi.org/10.1016/j.chemolab.2014.07.013.
Zhu, D., et al., 2019. P H Y S I C S Training of quantum circuits on a hybrid quantum computer [Online]. Available: https://www.science.org.